nanomaterials

MDPI

Article

Ag_2CO_3 Decorating BiOCOOH Microspheres with Enhanced Full-Spectrum Photocatalytic Activity for the Degradation of Toxic Pollutants

Shijie Li [1,*], Liuye Mo [1], Yanping Liu [2,*], Huiqiu Zhang [1], Yaming Ge [1] and Yingtang Zhou [1]

[1] Key Laboratory of Key Technical Factors in Zhejiang Seafood Health Hazards, Institute of Innovation & Application, Zhejiang Ocean University, Zhoushan 316022, China; liuyemo@zjou.edu.cn (L.M.); zhanghuiqiu2006@163.com (H.Z.); geyaming@126.com (Y.G.); zhouyingtang@zjou.edu.cn (Y.Z.)

[2] Department of Environmental Engineering, Zhejiang Ocean University, Zhoushan 316022, China

* Correspondence: lishijie@zjou.edu.cn (S.L); liuyp@zjou.edu.cn (Y.L.); Tel.: +86-21-6779-2557 (S.L)

Received: 6 October 2018; Accepted: 5 November 2018; Published: 7 November 2018

Abstract: The development of excellent full-spectrum photocatalysts is of vital significance to its practical application in environmental remediation. Herein, flower-like Ag_2CO_3/BiOCOOH type I heterostructures were prepared via a facile method and exhibited powerful photocatalytic activity by removing various toxic pollutants (rhodamine B, methyl blue, and tetracycline hydrochloride) under simulated sunlight irradiation. The boosted photocatalytic performance is attributed to the expanded range of the absorption spectrum and alleviated separation rate of the photo-induced electrons and holes. The photoluminescence spectra and trapping experiment were applied to clarify the photocatalytic reaction mechanism of Ag_2CO_3/BiOCOOH. The holes and $\bullet O_2^-$ were detected as the dominant reactive species involved in pollutant degradation. This work provides a novel full-spectrum-driven photocatalyst of Ag_2CO_3/BiOCOOH, which could effectively degrade toxic pollutants under simulated sunlight.

Keywords: Ag_2CO_3/BiOCOOH; heterojunction; photocatalysis; pollutant removal; full-spectrum

1. Introduction

Over the past few decades, toxic contaminants (e.g., industrial dyes and antibiotics) in water discharged by chemical industries have caused serious environmental pollution. However, conventional water treatment cannot efficiently degrade the contaminants. The application of photocatalytic technology in treating environmental pollution is regarded as an eco-friendly and sustainable technology to afford organic contaminant degradation [1–3]. The exploration of a novel full-spectrum-driven photocatalyst that can make the best use of sunlight has an important value in its practical application. Recently, great attention has been paid to Bi-based photocatalysts [4–11]. Among them, BiOCOOH is a kind of layered Bi-based oxide, built from $[Bi_2O_2]^{2+}$ fluorite-like layers intercalating by formic acid [12,13]. As an active ultraviolet-light-driven (ULD) photocatalyst, BiOCOOH possesses some advantages such as high chemical stability, a strong photo-redox driving force, and decent activity. However, the wide band gap (E_g = 3.4 eV) of BiOCOOH severely restrains its practical application. Actually, the combination of wide band gap semiconductors with narrow band gap compounds can remarkably enhance the photocatalytic performance, due to expanded sunlight absorption and the accelerated separation of charge carriers [14–18]. For instance, Aguirre et al. have recently employed Cu_2O coated by TiO_2 for improving photocatalytic stability and performance [16]. As a result, BiOCOOH was coupled with Ag_2O [19], CNT [20], RGO [21], C_3N_4 [22], BiOI [23], CQDs [24] and so on. Of note, the further exploration of fascinating full-spectrum-driven BiOCOOH-based heterojunction photocatalysts is still challenging.

Ag_2CO_3, as a highly active visible-light-driven photocatalyst, has been recognized as a good photosensitizer, since its narrow band gap (~2.17 V) is advantageous for sunlight absorption [25–27]. Hence, the design of Ag_2CO_3-based heterojunction photocatalysts (e.g., Ag_2CO_3/Ag_2O [28], Ag_2CO_3/Ag_2S [29], Ag_2CO_3/Bi_2MoO_6 [8,30], Ag_2CO_3/BiOCl [31], $Ag_2CO_3/Ag/WO_3$ [32] and Ag_2CO_3/AgBr/ZnO [33]) to improve the visible-light photocatalytic performance has been achieved by scholars. However, to the best of our knowledge, no Ag_2CO_3/BiOCOOH heterojunctions have been studied. Hence, it inspires us to combine BiOCOOH with Ag_2CO_3 for obtaining novel Ag_2CO_3/BiOCOOH heterojunctions with outstanding sunlight-driven photocatalytic performance.

In this study, aiming at the construction of highly active sunlight-driven photocatalysts, flower-like Ag_2CO_3/BiOCOOH heterojunctions were prepared via a simple precipitation approach. Under simulated sunlight irradiation, the photocatalytic property of Ag_2CO_3/BiOCOOH in the removal of various toxic pollutants (rhodamine B (RhB), methyl blue (MB), and tetracycline hydrochloride (TC)) was evaluated. In addition, the photocatalytic mechanism of Ag_2CO_3/BiOCOOH was also illustrated based on the experimental results.

2. Materials and Methods

2.1. Chemicals

$Bi(NO_3)_3 \bullet 5H_2O$, rhodamine B (RhB), $NaHCO_3$, $NH_3 \bullet H_2O$, glycerol, methyl blue (MB), ammonium oxalate (AO), tetracycline hydrochloride (TC), *N*,*N*-dimethylformamide (DMF), iso-propanol (IPA), and *p*-benzoquinone (BQ) were purchased from the Chinese Chemical Reagent factory and used as was received without further treatment.

2.2. Synthesis of Catalysts

BiOCOOH microspheres were prepared solvothermally. Typically, $Bi(NO_3)_3 \bullet 5H_2O$ (4 mmol) is dissolved in 50 mL of glycerol under vigorous stirring. After dissolution, 20 mL of DMF and 10 mL of H_2O were added into the above solution and stirred for 0.5 h. The obtained solution was poured into an autoclave with a volume of 100 mL and solvothermally treated at 160 °C for 24 h. After the reaction ended, the products collected from the suspension were washed with deionized water and ethanol four times, and finally transferred into an oven to get dried at 60 °C for 15 h.

Flower-like Ag_2CO_3/BiOCOOH heterojunctions were fabricated by chemical deposition. Firstly, a certain amount of BiOCOOH was evenly dispersed in 50 mL of deionized water during magnetic stirring. Subsequently, 1 mmol $AgNO_3$ was dissolved in the above system during magnetic stirring. Then, 10 mL of $NaHCO_3$ solution (0.05 M) was dropped into the above system slowly and stirred for another 2 h in darkness. Following this, the precipitant was washed thoroughly, and dried at 60 °C for 6 h. By changing the addition amount of BiOCOOH, the Ag_2CO_3/BiOCOOH heterojunctions with different mass ratios (0.3/1, 0.5/1, 1/1 and 1.5/1) were prepared and labelled as ACO/BOCH-30, ACO/BOCH-50, ACO/BOCH-100, and ACO/BOCH-150, respectively.

2.3. Characterization

X-ray powder diffraction (XRD) was conducted on a Bruker D8 Advance diffractometer (Cu Kα = 1.5406 Å) with a scanned range of 2θ from 10° to 80° (Karlsruhe, Germany). Scanning electron microscope (SEM, Hitachi S–4800, accelerating voltage = 10 kV, Tokyo, Japan), energy dispersive X-ray spectroscopy (EDX) (Berlin, Germany), and transmission electron microscope (TEM, JEM–2010F, Tokyo, Japan) were employed to study the morphologies and compositions of the catalysts. The UV-vis diffused reflectance spectra (DRS) were collected on a spectrophotometer (Shimadzu UV-2600, Tokyo, Japan). Room-temperature photoluminescence (PL) spectra were detected by using a Hitachi F-7000 fluorescence spectrophotometer (Tokyo, Japan).

2.4. Photocatalytic Performance Tests

The photo-degradation of rhodamine B (RhB), methyl blue (MB) or tetracycline hydrochloride (TC) under simulated sunlight was performed to assess the activity of catalysts. Briefly, 30 mg of catalyst was dispersed evenly in 100 mL of RhB (10 mg/L), MB (10 mg/L), or TC (20 mg/L) solution while magnetically stirring for 30 min in the dark to establish an adsorption-desorption equilibrium [34,35]. The reaction system was maintained at room temperature by using circulating water. Subsequently, the above system was illuminated by a 300 W xenon lamp with an average light intensity of 4.56 KW/m^2. During illumination, approximately 2 mL of the suspensions were sampled at certain intervals, and then centrifuged to get the supernatant solutions. The concentrations of solutions were quantified by using a UV-2600 spectrophotometer. Total organic carbon (TOC) experiments were carried out by the decomposition of RhB (50 mg/L, 200 mL) solution over 200 mg of ACO/BOCH-100 under simulated sunlight. The reaction solution collected at given intervals was detected by a Shimadzu TOC-VCPH TOC analyzer. To test the stability and reusability of ACO/BOCH-100, six successive runs for RhB degradation were performed, and each run lasted 30 min. After one cycle of photocatalytic reaction, the catalysts recycled by centrifugation and were washed thoroughly with deionized water and dried at 70 °C overnight. Subsequently, the dried catalysts were used to degrade the RhB solution again. During the recycling process, about 4.7 mg of the catalyst was lost.

3. Results and Discussion

3.1. Characterization

A series of Ag_2CO_3/BiOCOOH heterojunctions with various mass ratios (0.3/1, 0.5/1, 1/1, and 1.5/1) were fabricated and symbolized as ACO/BOCH-30, ACO/BOCH-50, ACO/BOCH-100, and ACO/BOCH-150, respectively. The crystallographic structures of as-prepared BiOCOOH, Ag_2CO_3, and Ag_2CO_3/BiOCOOH heterojunctions (ACO/BOCH-30, ACO/BOCH-50, ACO/BOCH-100, and ACO/BOCH-150) were studied by XRD (Figure 1). The diffraction peaks of BiOCOOH and Ag_2CO_3 coincided well with those of tetragonal BiOCOOH (JCPDS 35-0939) [13] and monoclinic Ag_2CO_3 (JCPDS 26-0399) [25,26], respectively. The XRD patterns of Ag_2CO_3/BiOCOOH heterojunctions display that both Ag_2CO_3 and BiOCOOH phases were detected in these heterojunctions, confirming the co-existence of Ag_2CO_3 and BiOCOOH in these as-prepared heterojunctions. Additionally, no trace of any impurity phase was detected.

The morphologies of BiOCOOH and the Ag_2CO_3/BiOCOOH heterojunction (ACO/BOCH-100) were visualized by SEM and TEM (Figure 2 and Figure S1). Pure BiOCOOH presented a flower-like structure (diameter: 1.5-2.5 μm), which was composed of numerous nanoplates (Figure S1). After its combination with Ag_2CO_3, the obtained Ag_2CO_3/BiOCOOH (ACO/BOCH-100) displayed a similar morphology to the BiOCOOH (Figure 2a). Further magnification of the image as presented in Figure 2b revealed that Ag_2CO_3 nanoparticles (size: 30-150 nm) were anchored onto the BiOCOOH microsphere. Further observation through TEM imaging (Figure 2c,d) confirmed that ACO/BOCH-100 was a flower-like architecture decorated by Ag_2CO_3 nanoparticles, verifying the successful fabrication of Ag_2CO_3/BiOCOOH with an intimately contacted interface. Furthermore, as shown in the energy dispersive spectroscopy (EDS) spectra, Ag, C, O, and Bi in ACO/BOCH-100 could be detected, testifying that the sample was Ag_2CO_3/BiOCOOH (Figure 3).

The surface texturing of BiOCOOH and ACO/BOCH-100 were analyzed by the N_2 adsorption–desorption isotherms (Figure S2). The BET specific surface areas of BiOCOOH and ACO/BOCH-100 were 26.2 and 22.7 m^{-2} g^{-1}, respectively. The BJH pore-size distributions revealed the presence of nanopores with the main pore size of 31 nm in BiOCOOH and ACO/BOCH-100 (the inset of Figure S2).

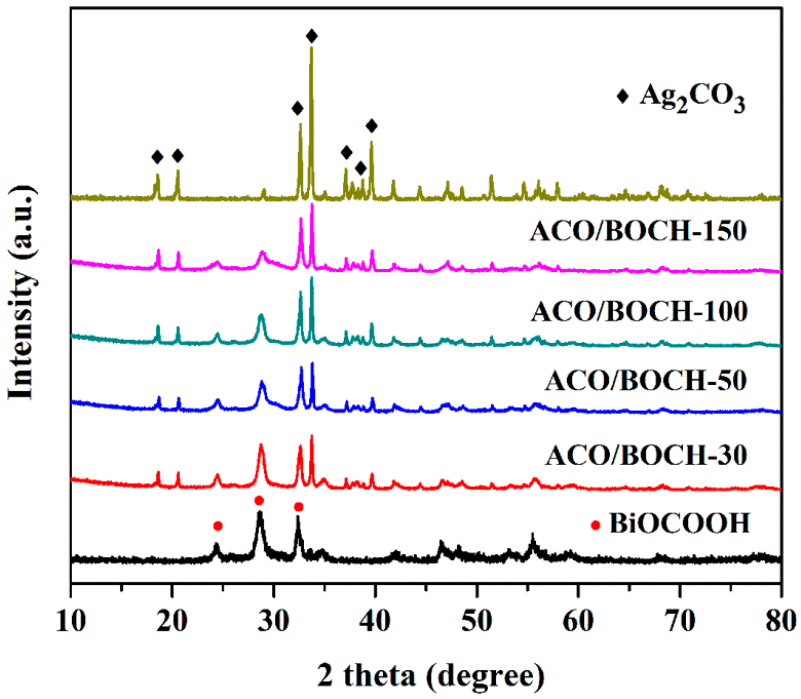

Figure 1. XRD patterns of pure BiOCOOH, Ag_2CO_3, and Ag_2CO_3/BiOCOOH heterojunctions (ACO/BOCH-30, ACO/BOCH-50, ACO/BOCH-100, and ACO/BOCH-150).

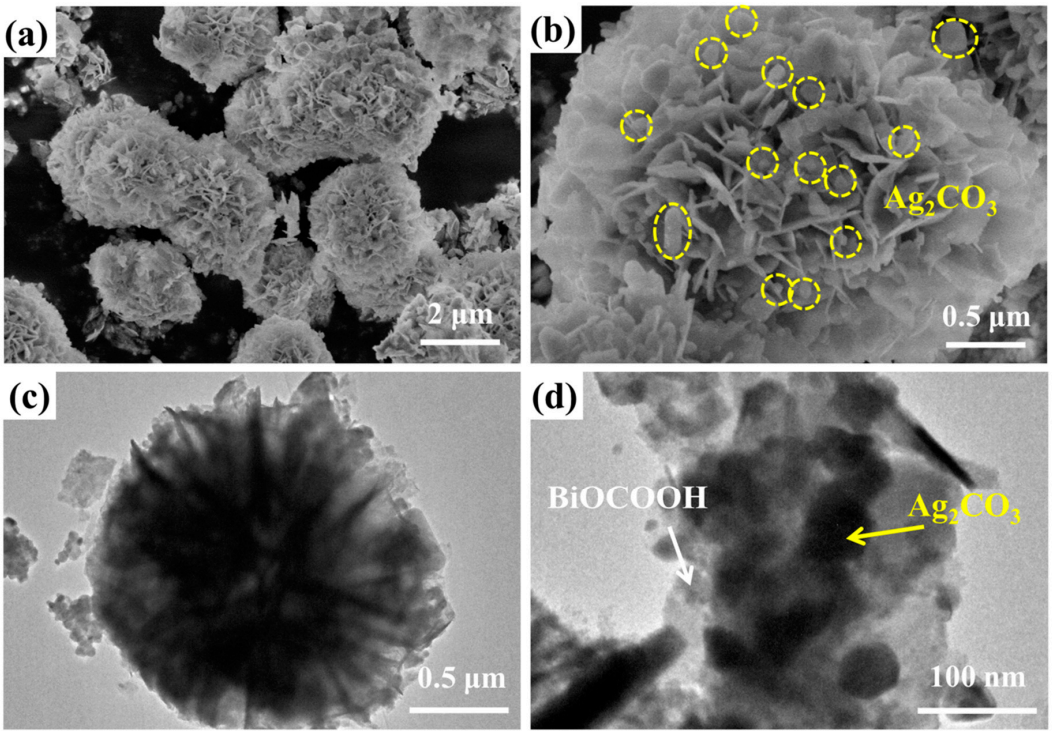

Figure 2. (**a**,**b**) SEM and (**c**,**d**) TEM images of ACO/BOCH-100.

The optical absorption behaviors of BiOCOOH, Ag_2CO_3, and Ag_2CO_3/BiOCOOH heterojunctions (ACO/BOCH-30, ACO/BOCH-50, ACO/BOCH-100, and ACO/BOCH-150) were studied by UV-vis diffuse reflectance spectrum (UV-vis DRS). As shown in Figure 4a, Ag_2CO_3 displayed intense absorbance in the VL region, whereas BiOCOOH had absorbance in the ultraviolet (UV) light region. The absorption band edges of pristine Ag_2CO_3 and BiOCOOH were about 470 and 365 nm, respectively, in agreement with previously reported results. The light absorption near the band edge followed the

Tauc equation: $\alpha h\nu = A\ (h\nu - E_g)^{n/2}$, where α, h, ν, and A were the absorption coefficient, Planck's constant, light frequency, and the constant, respectively. According to the calculated Tauc's plot (Figure S3), the band gaps (E_g) of Ag_2CO_3 and BiOCOOH were 2.17 and 3.40 eV, in accordance with the results previously reported [8,23,32].

The conduction band (CB) and valence band (VB) potentials of BiOCOOH and Ag_2CO_3 were calculated by the empirical equations:

$$E_{VB} = X - E_0 + 0.5E_g \quad (1)$$

$$E_{CB} = E_{VB} - E_g \quad (2)$$

where the X is the absolute electronegativity of the semiconductor, the E_0 value equals to ~4.5 eV, E_g is the band gap of the semiconductor. Based on the equations above, the E_{CB} and E_{VB} of BiOCOOH were estimated to be -0.67 and 2.73 eV, and those of Ag_2CO_3 were calculated as 0.43 and 2.60 eV.

The photoluminescence (PL) was measured to investigate the separation efficiency of electrons and holes [36–39]. Figure 4b presents the PL spectra of BiOCOOH and ACO/BOCH-100. Clearly, BiOCOOH had a strong emission peak centered at around 370 nm. The PL emission peak of ACO/BOCH-100 was weaker than that of bare BiOCOOH, signifying that the recombination of carriers was pronouncedly reduced.

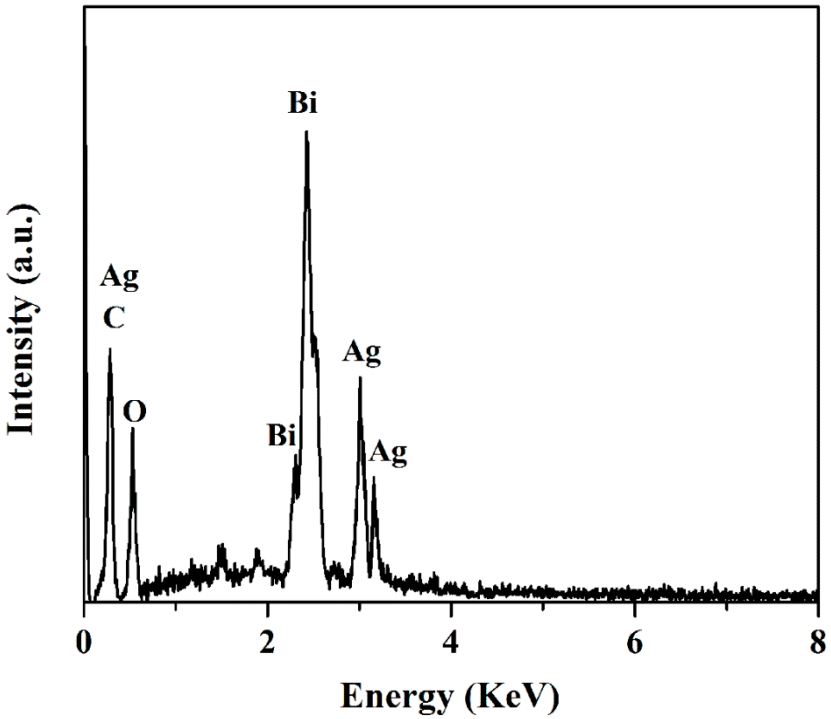

Figure 3. EDS spectra of ACO/BOCH-100.

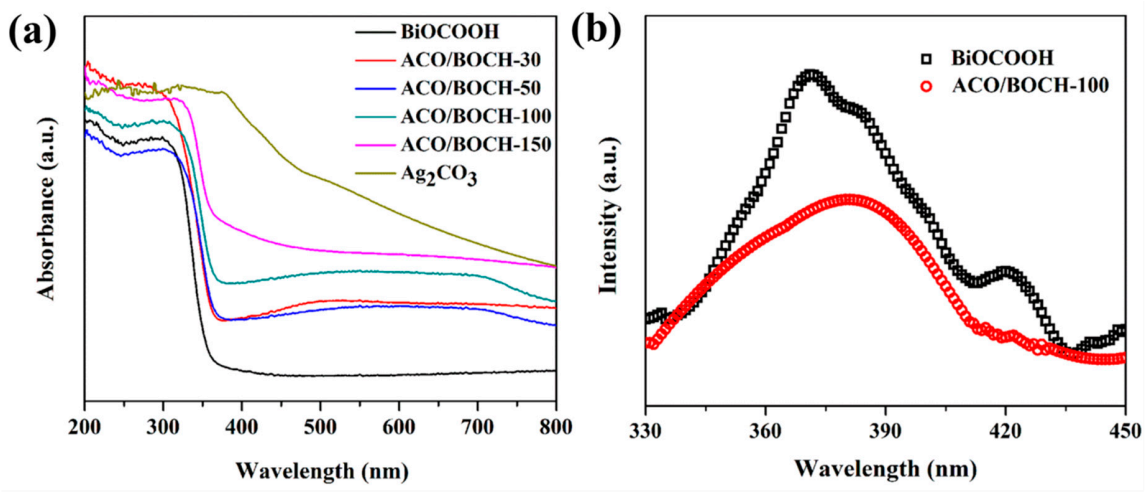

Figure 4. (**a**) UV-vis DRS of pure BiOCOOH, Ag_2CO_3, and Ag_2CO_3/BiOCOOH heterojunctions (ACO/BOCH-30, ACO/BOCH-50, ACO/BOCH-100, and ACO/BOCH-150). (**b**) PL spectra of pure BiOCOOH and ACO/BOCH-100 with an excitation wavelength of 300 nm.

3.2. Photocatalytic Performance

The photocatalytic performances of Ag_2CO_3/BiOCOOH were assessed by degrading industrial dyes (RhB and MB), and antibiotic (TC) under simulated sunlight. Figure 5a presents the RhB degradation curves with various catalysts. No RhB was degraded in the absence of catalysts. The RhB degradation efficiency by using BiOCOOH, Ag_2CO_3 or Ag/Ag_2CO_3 reached 31.3%, 98.7% or 100% in 60 min of reaction. As BiOCOOH combined with Ag_2CO_3, the activity of these heterojunctions was pronouncedly enhanced and much higher than pure BiOCOOH. Among these Ag_2CO_3/BiOCOOH heterojunctions, ACO/BOCH-100 showed the highest photocatalytic activity with 100% of RhB degraded within 30 min, which was much higher than using Ag_2CO_3/Ag (76.1%), or Ag_2CO_3 (60.8%). To illustrate the synergistic effect between Ag_2CO_3 and BiOCOOH, the RhB photodegradation efficiency using the mechanical mixture (50 wt% Ag_2CO_3 + 50 wt% BiOCOOH) as the catalyst, was tested, which was much lower than that achieved by using ACO/BOCH-100, revealing that the formation of the Ag_2CO_3/BiOCOOH heterojunction can effectively boost the photocatalytic performance. Notably, the content of Ag_2CO_3 in the heterojunction played a significant role in enhancing the photocatalytic performance of as-prepared samples. However, when the loading amount of Ag_2CO_3 was high (ACO/BOCH-150), BiOCOOH was decorated by excessive Ag_2CO_3 nanoparticles with a relatively larger size, resulting in decreased photocatalytic activity.

Figure 5b shows the degradation curves of RhB with the reaction time in the presence of ACO/BOCH-100. Obviously, the major absorption peak at 554 nm rapidly decreased as the reaction time prolonged, indicating the decomposition of the structure. After 30 min of reaction, 100% of RhB was degraded, demonstrating the distinguished photocatalytic activity of ACO/BOCH-100 under simulated sunlight.

The reaction kinetics of RhB degradation over various catalysts was further studied. The experimental data could be fitted well with the pseudo-first-order model (Figure S4). It was found that ACO/BOCH-100 had the highest rate constant value of 0.1335 min^{-1}, approximately 22.6, 2.1, or 5.2 folds that of pristine BiOCOOH (0.0059 min^{-1}), Ag_2CO_3 (0.0638 min^{-1}), or the mixture (0.0258 min^{-1}).

MB dye and TC antibiotic, two refractory contaminants were also used to further investigate the photocatalytic activity of Ag_2CO_3/BiOCOOH under simulated sunlight (Figure 6, Figures S5 and S6). Notably, the MB degradation efficiency gained by employing ACO/BOCH-100 was as high as 100% within 60 min of irradiation, markedly higher than that gained by employing pristine BiOCOOH (42.7%), Ag_2CO_3 (79.3%), Ag/Ag_2CO_3 (89.7%), or a mechanical mixture (70.4%) as the photocatalyst. Additionally, a similar phenomenon was observed when using TC (Figure 6 and Figure S6) as a

model contaminant. The optimal ACO/BOCH-100 possessed high photocatalytic activity with a TC degradation efficiency of 93.4% in 120 min, much greater than those of pure BiOCOOH (31.8%), Ag_2CO_3 (60.3%), Ag/Ag_2CO_3 (67.2%), as well as their physical mixture (52.3%). The results indicated that Ag_2CO_3/BiOCOOH had no-selectivity and could effectively decompose various toxic pollutants under simulated sunlight.

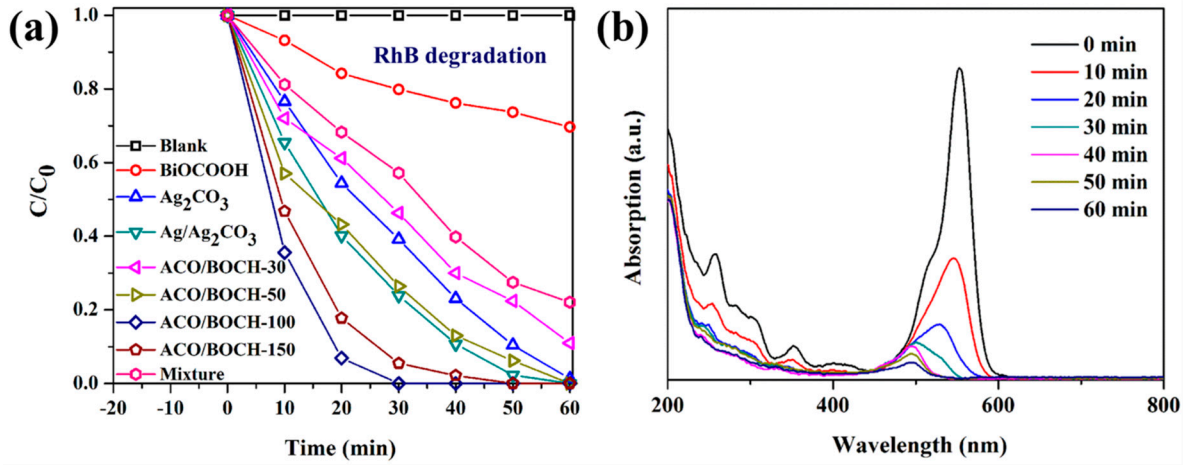

Figure 5. (**a**) Photocatalytic degradation of RhB dye with various catalysts under simulated sunlight. (**b**) Absorption spectra of RhB with irradiation time in the presence of ACO/BOCH-100.

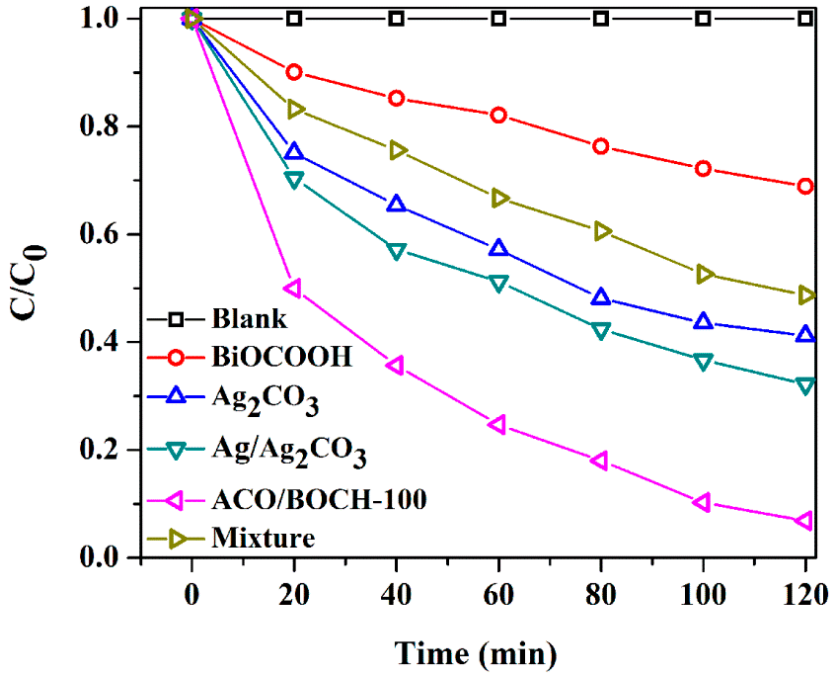

Figure 6. Photocatalytic degradation of TC with different catalysts under simulated sunlight.

The photocatalytic performances of other reported catalysts for RhB removal were listed in Table S1. Notably, our catalyst showed a higher removal rate than other catalysts with similar/higher dosage of catalyst. Therefore, the Ag_2CO_3/BiOCOOH heterojunction possesses an excellent photocatalysis property for removing organic pollutants under simulated sunlight.

The mineralization ability of a catalyst is vital for its practical application [40,41]. Therefore, the TOC values during the degradation of RhB (150 mL, 50 mg L^{-1}) over ACO/BOCH-100 (200 mg) were determined. As shown in Figure 7a, 83.7% of TOC was removed after 5 h of irradiation, indicating that ACO/BOCH-100 holds a huge potential for the deep treatment of toxic contaminants.

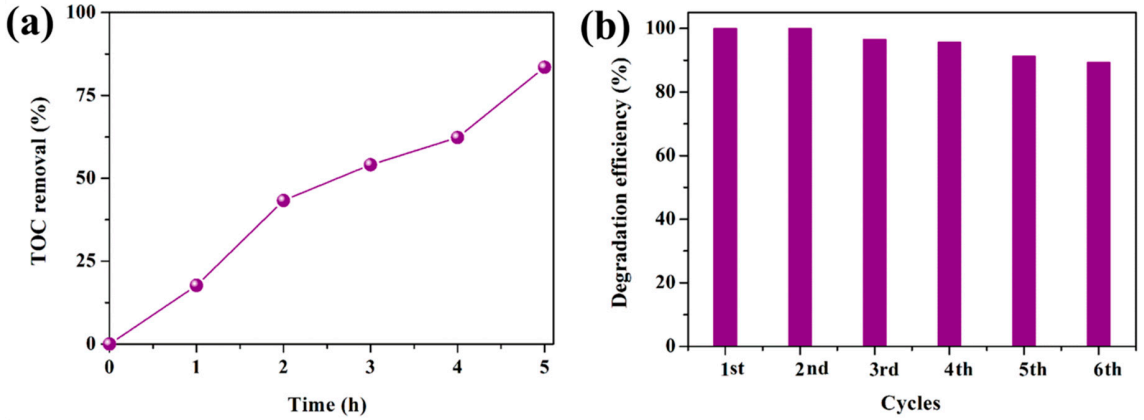

Figure 7. (**a**) TOC removal efficiencies over ACO/BOCH-100. (**b**) Cycling runs in the removal of RhB dye over ACO/BOCH-100.

The reusability of ACO/BOCH-100 was investigated via recycling for six runs in the removal of RhB and each run lasted 30 min. Figure 7b shows the photocatalytic performance of recycled ACO/BOCH-100. It was observed that the degradation efficiency of RhB at 30 min of the sixth run was 89.2%, which showed no apparent decrease compared with that (100%) of the first run, demonstrating the good stability of ACO/BOCH-100. During the photocatalytic process, it was found that there was a mass loss of 30 mg for the first run to 25.3 mg for the sixth run. Thus, the slight decline in activity should be attributed to the loss of catalysts during the recycling process. Moreover, the XRD characterization has demonstrated the formation of Ag_2CO_3/Ag after recycling experiments (Figure S7), which has been recognized as a stable hetero-structure [25,32]. These results indicate that ACO/BOCH-100 belongs to a type of stable catalysts.

3.3. Photocatalytic Mechanism

Radical trapping experiments were conducted to investigate the effect of reactive species on the degradation of RhB over Ag_2CO_3/BiOCOOH [3,30,42]. As indicated in Figure 8, the RhB degradation efficiency reached 100% in the absence of a quencher. With the introduction of isopropanol (IPA), benzoquinone (BQ) and ammonium oxalate (AO), the photocatalytic activity of ACO/BOCH-100 was greatly suppressed, with RhB degradation efficiencies of 87.9%, 65.7% and 49.8%, respectively. The results demonstrated that •OH, $\bullet O_2^-$ and h^+ were generated during photocatalysis, and $\bullet O_2^-$ and h^+ were mainly responsible for RhB degradation over Ag_2CO_3/BiOCOOH.

On the basis of the results from systematic characterizations, the possible photocatalytic mechanism for contaminant degradation over Ag_2CO_3/BiOCOOH under simulated sunlight was proposed as outlined in Figure 9. Electrons and holes are produced in Ag_2CO_3 and BiOCOOH under simulated sunlight. Afterwards, the photo-generated electrons on CB and holes on VB of BiOCOOH tend to transfer to those of Ag_2CO_3 accordingly. Such a transfer process is beneficial to the separation of electrons and holes [43], as verified by the PL characterization (Figure 4b). Additionally, the photoelectrons can drift to the surface of Ag_2CO_3, leading to the formation of metallic Ag via the reduction of partial Ag^+ (Ag_2CO_3). The produced metallic Ag can further facilitate electron migration to retard the recombination of charge carriers [44]. Finally, the electrons stored on the CB of metallic Ag can react with O_2 to yield $\bullet O_2^-$ radicals, which can be consumed to degrade toxic pollutants (RhB/MB/TC). Meanwhile, the holes that have accumulated on the VB of Ag_2CO_3 are involved in the degradation of toxic contaminants. Apparently, the results illustrate that the construction of type I heterojunction between Ag_2CO_3 and BiOCOOH can facilitate the separation of charge carriers, further improving the photocatalytic performance.

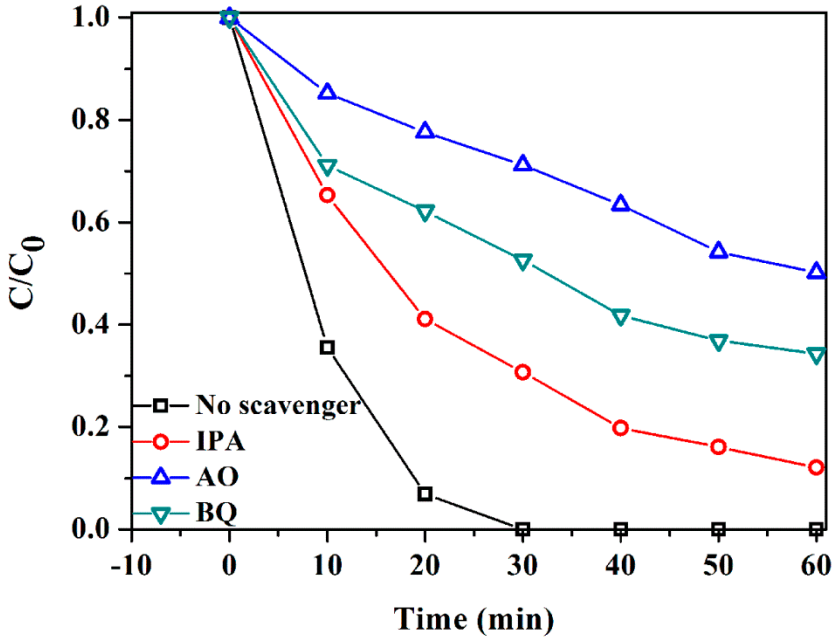

Figure 8. Radical–scavenge tests in the removal of RhB in the presence of ACO/BOCH-100.

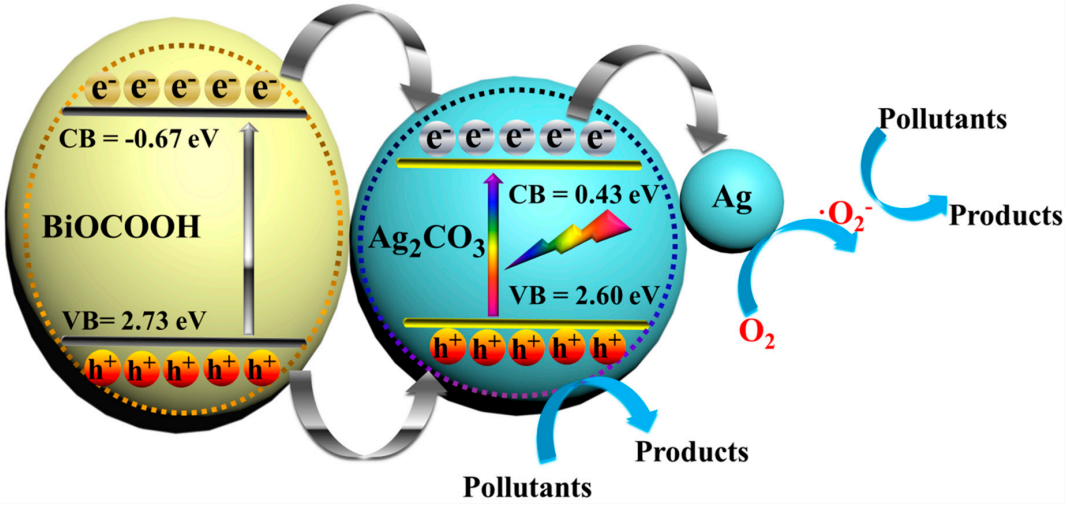

Figure 9. Proposed mechanism of pollutant removal over Ag_2CO_3/BiOCOOH under simulated sunlight.

4. Conclusions

Ag_2CO_3 nanoparticles interspersed-BiOCOOH heterojunction photocatalytsts were prepared by a facile procedure. In comparison with pure Ag_2CO_3 and BiOCOOH, Ag_2CO_3/BiOCOOH (ACO/BOCH-100) exhibited superior photocatalytic activity for the degradation of toxic pollutants (RhB, MB, and TC) under simulated sunlight. The synergy effect between Ag_2CO_3 and BiOCOOH not only expanded the sunlight absorption range but also promoted the separation of electron and holes, leading to the outstanding performance of Ag_2CO_3/BiOCOOH. This novel photocatalyst can be employed to degrade refractory pollutants under simulated sunlight.

Supplementary Materials: The following are available online at http://www.mdpi.com/2079-4991/8/11/914/s1, Figure S1: SEM image of pristine BiOCOOH, Figure S2: N_2 adsorption-desorption isotherms of BiOCOOH and ACO/BOCH-100. The inset is the corresponding pore-size distributions, Figure S3: The Tauc plots of BiOCOOH and Ag_2CO_3, Figure S4: Pseudo-first-order kinetic plots and rate constants of RhB degradation over various photocatalysts, Figure S5: The MB degradation curves over different samples, Figure S6: Absorption spectra of TC with irradiation time in the presence of ACO/BOCH-100, Figure S7: The XRD patterns of ACO/BOCH-100 before and after cycling tests, Table S1: Summary of reported photocatalysts for degradation of RhB.

Author Contributions: S.L.: idea, and design of the paper; performed the tests; analyzed the data; wrote this paper. Y.L., H.Z., L.M., Y.G. and Y.Z. assisted the characterizations.

Funding: This work has been financially supported by the National Natural Science Foundation of China (51708504), the Public Projects of Zhejiang Province (LGN18E080003), and the Science and Technology Project of Zhoushan (2017C41006).

Conflicts of Interest: The authors declare no conflicts of interest.

References

1. Zhu, S.S.; Wang, D.W. Photocatalysis: Basic principles, diverse forms of implementations and emerging scientifc opportunities. *Adv. Energy Mater.* **2017**, *7*, 1700841. [CrossRef]
2. Li, S.; Shen, X.; Liu, J.; Zhang, L. Synthesis of Ta_3N_5/Bi_2MoO_6 core-shell fiber-shaped heterojunctions as efficient and easily recyclable photocatalysts. *Environ. Sci. Nano* **2017**, *4*, 1155–1167. [CrossRef]
3. Li, S.; Hu, S.; Xu, K.B.; Jiang, W.; Liu, J.; Wang, Z. A novel heterostructure of BiOI nanosheets anchored onto MWCNTs with excellent visible-light photocatalytic activity. *Nanomaterials* **2017**, *7*, 22. [CrossRef] [PubMed]
4. Yang, Y.; Zhang, C.; Lai, C.; Zeng, G.; Huang, D.; Cheng, M.; Wang, J.; Chen, F.; Zhou, C.; Xiong, W. BiOX (X = Cl, Br, I) photocatalytic nanomaterials: Applications for fuels and environmental management. *Adv. Colloid Interface* **2018**, *254*, 76–93. [CrossRef] [PubMed]
5. Li, S.; Hu, S.; Jiang, W.; Liu, Y.; Zhou, Y.; Liu, Y.; Mo, L. Hierarchical architectures of bismuth molybdate nanosheets onto nickel titanate nanofibers: Facile synthesis and efficient photocatalytic removal of tetracycline hydrochloride. *J. Colloid Interface Sci.* **2018**, *521*, 42–49. [CrossRef] [PubMed]
6. Lu, Y.; Huang, Y.; Zhang, Y.; Cao, J.-j.; Li, H.; Bian, C.; Lee, S.C. Oxygen vacancy engineering of $Bi_2O_3/Bi_2O_2CO_3$ heterojunctions: Implications of the interfacial charge transfer, NO adsorption and removal. *Appl. Catal. B* **2018**, *231*, 357–367. [CrossRef]
7. Zhang, J.L.; Ma, Z.J. Flower-like Ag_2MoO_4/Bi_2MoO_6 heterojunctions with enhanced photocatalytic activity under visible light irradiation. *Taiwan Inst. Chem. Eng.* **2017**, *71*, 156–164. [CrossRef]
8. Li, S.; Jiang, W.; Hu, S.; Liu, Y.; Liu, Y.; Xu, K.; Liu, J. Hierarchical heterostructure of Bi_2MoO_6 micro-flowers decorated with Ag_2CO_3 nanoparticles for efficient visible-light-driven photocatalytic removal of toxic pollutants. *Beilstein J. Nanotechnol.* **2018**, *9*, 2297–2305. [CrossRef] [PubMed]
9. Xu, B.; An, Y.; Liu, Y.; Qin, X.; Zhang, X.; Dai, Y.; Wang, Z.; Wang, P.; Whangbo, M.-H.; Huang, B. Enhancing the photocatalytic activity of BiOX (X = Cl, Br, I), $(BiO)_2CO_3$ and Bi_2O_3 by modifying their surfaces with polar organic anions, 4-substituted thiophenolates. *J. Mater. Chem. A* **2017**, *5*, 14406–14414. [CrossRef]
10. Ganose, A.M.; Cuff, M.; Butler, K.T.; Scanlon, D.O. Interplay of orbital and relativistic effects in bismuth oxyhalides: BiOF, BiOCl, BiOBr, and BiOI. *Chem. Mater.* **2016**, *28*, 1980–1984. [CrossRef] [PubMed]
11. Liang, C.; Niu, C.; Wen, X.; Yang, S.; Guo, H.; Zeng, G.-M. Construction of 2D heterojunction system with enhanced photocatalytic performance: Plasmonic Bi and reduced graphene oxide co-modified Bi_5O_7I with high-speed charge transfer channels. *J. Hazard Mater.* **2018**, *361*, 245–258. [CrossRef] [PubMed]
12. Xiong, J.Y.; Cheng, G.; Lu, Z.; Tang, J.L.; Yu, X.L.; Chen, R. BiOCOOH hierarchical nanostructures: Shape-controlled solvothermal synthesis and photocatalytic degradation performances. *CrystEngComm* **2011**, *13*, 2381–2390. [CrossRef]
13. Duan, F.; Zheng, Y.; Liu, L.; Chen, M.Q.; Xie, Y. Synthesis and photocatalytic behaviour of 3D flowerlike bismuth oxide formate architectures. *Mater. Lett.* **2010**, *64*, 1566–1569. [CrossRef]
14. Ye, R.; Zhao, J.; Wickemeyer, B.B.; Toste, F.D.; Somorjai, G.A. Foundations and strategies of the construction of hybrid catalysts for optimized performances. *Nat. Catal.* **2018**, *1*, 318–325. [CrossRef]
15. Wu, M.J.; Wu, J.Z.; Zhang, J.; Chen, H.; Zhou, J.Z.; Qian, G.R.; Xu, Z.P.; Du, Z.; Rao, Q.L. A review on fabricating heterostructures from layered double hydroxides for enhanced photocatalytic activities. *Catal. Sci. Technol.* **2018**, *8*, 1207–1228. [CrossRef]
16. Aguirre, M.E.; Zhou, R.; Eugene, A.J.; Guzman, M.I.; Grela, M.A. Cu_2O/TiO_2 heterostructures for CO_2 reduction through a direct Z-scheme: Protecting Cu_2O from photocorrosion. *Appl. Catal. B* **2017**, *217*, 485–493. [CrossRef]
17. Li, S.; Jiang, W.; Xu, K.; Hu, S.; Liu, Y.; Zhou, Y.; Liu, J. Synthesis of flower-like AgI/BiOCOOH p-n heterojunctions with enhanced visible-light photocatalytic performance for the removal of toxic pollutants. *Front. Chem.* **2018**, *6*, 518. [CrossRef]

18. Li, S.; Liu, Y.; Long, Y.; Mo, L.; Zhang, H.; Liu, J. Facile synthesis of Bi_2MoO_6 microspheres decorated by CdS nanoparticles with efficient photocatalytic removal of levfloxacin antibiotic. *Catalysts* **2018**, *8*, 477. [CrossRef]
19. Li, S.J.; Xu, K.B.; Hu, S.W.; Jiang, W.; Zhang, J.L.; Liu, J.S.; Zhang, L.S. Synthesis of flower-like Ag_2O/BiOCOOH p-n heterojunction with enhanced visible light photocatalytic activity. *Appl. Surf. Sci.* **2017**, *397*, 95–103. [CrossRef]
20. Hu, S.W.; Li, S.J.; Xu, K.B.; Jiang, W.; Zhang, J.L.; Liu, J.S. MWCNTs/BiOCOOH composites with improved sunlight photocatalytic activity. *Mater. Lett.* **2017**, *191*, 157–160. [CrossRef]
21. Xia, S.-H.; Dong, C.; Wei, X.-W.; Wang, J.; Wu, K.-L.; Hu, Y.; Ye, Y. Reduced graphene oxide modified flower-like BiOCOOH architectures with enhanced photocatalytic activity. *Mater. Lett.* **2015**, *156*, 36–38. [CrossRef]
22. Cui, Y.; Zhang, X.; Zhang, H.; Cheng, Q.; Cheng, X. Construction of BiOCOOH/g-C_3N_4 composite photocatalyst and its enhanced visible light photocatalytic degradation of amido black 10B. *Sep. Purif. Technol.* **2019**, *210*, 125–134. [CrossRef]
23. Chai, B.; Wang, X. Enhanced visible light photocatalytic activity of BiOI/BiOCOOH composites synthesized via ion exchange strategy. *RSC Adv.* **2015**, *5*, 7589–7596. [CrossRef]
24. Chen, P.; Zhang, Q.; Su, Y.; Shen, L.; Wang, F.; Liu, H.; Liu, Y.; Cai, Z.; Lv, W.; Liu, G. Accelerated photocatalytic degradation of diclofenac by a novel CQDs/BiOCOOH hybrid material under visible-light irradiation: Dechloridation, detoxicity, and a new superoxide radical model study. *Chem. Eng. J.* **2018**, *332*, 737–748. [CrossRef]
25. Liu, Y.; Kong, J.J.; Yuan, J.L.; Zhao, W.; Zhu, X.; Sun, C.; Xie, J.M. Enhanced photocatalytic activity over flower-like sphere Ag/Ag_2CO_3/$BiVO_4$ plasmonic heterojunction photocatalyst for tetracycline degradation. *Chem. Eng. J.* **2018**, *331*, 242–254. [CrossRef]
26. Li, T.T.; Hu, X.L.; Liu, C.C.; Tang, C.M.; Wang, X.K.; Luo, S.L. Efficient photocatalytic degradation of organic dyes and reaction mechanism with Ag_2CO_3/$Bi_2O_2CO_3$ photocatalyst under visible light irradiation. *J. Mol. Catal. A Chem.* **2016**, *425*, 124–135. [CrossRef]
27. Yao, X.; Liu, X. One-pot synthesis of ternary Ag_2CO_3/Ag/AgCl photocatalyst in natural geothermal water with enhanced photocatalytic activity under visible light irradiation. *J. Hazard Mater.* **2014**, *280*, 260–268. [CrossRef] [PubMed]
28. Zhao, X.; Su, Y.; Qi, X.; Han, X. A facile method to prepare novel Ag_2O/Ag_2CO_3 three-dimensional hollow hierarchical structures and their water purification function. *ACS Sustain. Chem. Eng.* **2017**, *5*, 6148–6158. [CrossRef]
29. Yu, C.; Wei, L.; Zhou, W.; Dionysiou, D.D.; Zhu, L.; Shu, Q.; Liu, H. A visible-light-driven core-shell like Ag_2S@Ag_2CO_3 composite photocatalyst with high performance in pollutants degradation. *Chemosphere* **2016**, *157*, 250–261. [CrossRef] [PubMed]
30. Zhang, J.L.; Ma, Z. Ag-Ag_2CO_3/Bi_2MoO_6 composites with enhanced visible-light-driven catalytic activity. *J. Taiwan Inst. Chem. Eng.* **2018**, *71*, 156–164. [CrossRef]
31. Fang, S.S.; Ding, C.Y.; Liang, Q.; Li, Z.Y.; Xu, S.; Peng, Y.Y.; Lu, D.Y. In-situ precipitation synthesis of novel BiOCl/Ag_2CO_3 hybrids with highly efficient visible-light-driven photocatalytic activity. *J. Alloy. Compd.* **2016**, *684*, 230–236. [CrossRef]
32. Yuan, X.Z.; Jiang, L.B.; Chen, X.H.; Leng, L.J.; Wang, H.; Wu, Z.B.; Xiong, T.; Liang, J.; Zeng, G.M. Highly efficient visible-light-induced photoactivity of Z-scheme Ag_2CO_3/Ag/WO_3 photocatalysts for organic pollutant degradation. *Environ. Sci. Nano* **2017**, *4*, 2175–2185. [CrossRef]
33. Pirhashemi, M.; Habibi-Yangjeh, A. Photosensitization of ZnO by AgBr and Ag_2CO_3: Nanocomposites with tandem n-n heterojunctions and highly enhanced visible-light photocatalytic activity. *J. Colloid Interface Sci.* **2016**, *474*, 103–113. [CrossRef] [PubMed]
34. Zhou, R.; Guzman, M.I. Photocatalytic Reduction of Fumarate to Succinate on ZnS Mineral Surfaces. *J. Phys. Chem. C* **2016**, *120*, 7349–7357. [CrossRef]
35. Zhou, R.; Guzman, M.I. CO_2 Reduction under Periodic Illumination of ZnS. *J. Phys. Chem. C* **2014**, *118*, 11649–11656. [CrossRef]
36. Ma, H.; Zhao, Y.; Souvanhthong, B.; Zhao, J. Time-dependent synthesis of BiO_{2-x}/Bi composites with efficient visible-light induced photocatalytic activity. *J. Colloid Interface Sci.* **2018**, *531*, 311–319. [CrossRef] [PubMed]

37. Li, S.; Hu, S.; Jiang, W.; Zhou, Y.; Liu, J.; Wang, Z. Facile synthesis of cerium oxide nanoparticles decorated flower-like bismuth molybdate for enhanced photocatalytic activity toward organic pollutant degradation. *J. Colloid Interface Sci.* **2018**, *530*, 171–178. [CrossRef] [PubMed]
38. Li, S.; Hu, S.; Jiang, W.; Liu, Y.; Liu, Y.; Zhou, Y.; Mo, L.; Liu, J. Ag_3VO_4 nanoparticles decorated $Bi_2O_2CO_3$ micro-flowers: An efficient visible-light-driven photocatalyst for the removal of toxic contaminants. *Front. Chem.* **2018**, *6*, 255. [CrossRef] [PubMed]
39. Zhang, K.; Wang, J.; Jiang, W.J.; Yao, W.Q.; Yang, H.P.; Zhou, Y.F. Self-assembled perylene diimide based supramolecular heterojunction with Bi_2WO_6 for efficient visible-light-driven photocatalysis. *Appl. Catal. B* **2018**, *232*, 175–181. [CrossRef]
40. Li, S.; Hu, S.; Zhang, J.; Jiang, W.; Liu, J. Facile synthesis of Fe_2O_3 nanoparticles anchored on Bi_2MoO_6 microflowers with improved visible light photocatalytic activity. *J. Colloid Interface Sci.* **2017**, *497*, 93–101. [CrossRef] [PubMed]
41. Wu, Z.; Yu, C.; Liu, R.; Dionysiou, D.D.; Yang, K.; Wang, C.; Liu, H. Novel fluorinated Bi_2MoO_6 nanocrystals for efficient photocatalytic removal of water organic pollutants under different light source illumination. *Appl. Catal. B* **2017**, *209*, 1–11.
42. Wang, Y.; Wang, H.; Xu, A.; Song, Z. Facile synthesis of Ag_3PO_4 modified with GQDs composites with enhanced visible-light photocatalytic activity. *J. Mater. Sci. Mater. Electron.* **2018**, *29*, 16691–16701. [CrossRef]
43. Wang, F.F.; Li, Q.; Xu, D.S. Recent Progress in Semiconductor-Based Nanocomposite Photocatalysts for Solar-to-Chemical Energy Conversion. *Adv. Energy Mater.* **2017**, *7*, 1700529. [CrossRef]
44. Chen, J.B.; Che, H.N.; Huang, K.; Liu, C.B.; Shi, W.D. Fabrication of a ternary plasmonic photocatalyst CQDs/Ag/Ag_2O to harness charge flow for photocatalytic elimination of pollutants. *Appl. Catal. B* **2016**, *192*, 134–144. [CrossRef]